Formulation of a 1D finite element of heat exchanger for accurate modelling of the grouting behaviour: Application to cyclic thermal loading

Cerfontaine, Benjamin; Radioti, Georgia; Collin, Frédéric; Charlier, Robert

Published in:
Renewable Energy

DOI:
10.1016/j.renene.2016.04.034

Publication date:
2016

Document Version
Peer reviewed version

Formulation of a 1D finite element of heat exchanger for accurate modelling of the grouting behaviour: application to cyclic thermal loading

B.Cerfontaine[a,*], G. Radioti[a,b], F. Collin[a], R. Charlier[a]

[a] *University of Liege, Geomechanics and Engineering Geology, Chemin des chevreuils, Liege, Belgium*
[b] *F.R.I.A., Fonds de la Recherche Scientifique - FNRS, Brussels, Belgium*

Abstract

This paper presents a comprehensive formulation of a finite element for the modelling of borehole heat exchangers. This work focuses on the accurate modelling of the grouting and the field of temperature near a single borehole. Therefore the grouting of the BHE is explicitly modelled. The purpose of this work is to provide tools necessary to the further modelling of thermo-mechanical couplings.
The finite element discretises the classical governing equation of advection-diffusion of heat within a 1D pipe connected to ground nodes. Petrov-Galerkin weighting functions are used to avoid numerical disturbances. The formulation is able to capture highly transient and steady-state phenomena.
The proposed finite element is validated with respect to analytical solutions. An example consisting of a 100m depth U-pipe is finally simulated. A first continuous heating simulation highlights the non-symmetric distribution of temperature inside and near the borehole. An estimation of the error on the results as a function of the resolution parameters is also carried out. Finally simulations of cyclic thermal loading exhibit the need to take into account all daily variations if the grouting behaviour must be modelled. This is true especially in case of freeze-thaw damaging risk.

Keywords: Borehole heat exchanger; Ground source heat pump; Finite element; Short-time step; Numerical modelling;

1. Introduction

Among the different possibilities that geothermal energy offers, energy extraction through geothermal heat pumps is the most frequent worldwide application and increasing over the last years [1]. Shallow geothermal heat pump systems exchange heat with the ground either by circulating the groundwater

[1] Contact email: b.cerfontaine@ulg.ac.be

through two separate wells (open-loop) or by using heat exchangers embedded in the ground mass (closed-loop). Vertical closed-loop geothermal systems, also known as Borehole Heat Exchangers (BHEs), are widely used since they have a small footprint at the surface for installation and can be applied in many hydrogeological contexts [2, 3]. BHEs consist typically of one or two loops of high-density polyethylene pipes installed in a borehole. A heat carrier fluid is circulated in the pipe loop and heat is transferred between the fluid and the surrounding ground. A grouting material is usually injected in the borehole to enhance the heat transfer between the circulating fluid and the surrounding ground and to prevent environmental risks. These systems are widely used for heating and cooling of buildings and small compounds [4]. In winter heat is extracted from the ground (heating of the building) while in summer heat is injected in the ground (cooling of the building).

The long-term use of BHE may have many technical and environmental consequences [5] such as the influence on groundwater quality or the reduction of efficiency of the injection/extraction process. Sustainability of BHE is a crucial issue [6]. This consists in finding the maximum level of energy production allowing a constant production for a very long time. Therefore the optimisation of single or fields of BHE is carried out in order to limit their impact or increase their efficiency [7, 8, 9]. Limitations of temperature variations within the soil, the carrier fluid and the grouting is another constraint. Indeed the freeze-thaw cycles may affect the thermal properties of the grouting [10, 11, 12] or the shallow aquifer quality [5]. The evaluation of these consequences requires the development of analytical and numerical models able to capture all the features of BHE-ground interactions.

Analytical and semi-analytical solutions are widely used for the BHE design and optimisation [7, 8, 9] especially due to their low computational cost. Early solutions are developed to analyse the long-term behaviour of BHE [13, 14]. They are limited to conduction only and drop vertical effects or pipe interactions. [15] extend one of these methods to take into account short-term behaviour which is proven important for some applications. The basic infinite line source, finite line source and infinite cylindrical source models are compared in [16] and their applicability is classified with respect to the duration of the simulation.

Refinements of analytical methods are more and more developed. Heat advection in the surrounding soil is taken into account in [17] despite the proposed solution is in 2D. The interaction between pipes is included in [18]. [19, 20] propose a model dealing with vertical conduction as well as advection-diffusion in the soil and discontinuous loading. A classification procedure of these models is proposed in [21].

Finally some other authors try to better estimate the variation of temperature within the pipe only in order to simplify the resistance parameter identification procedure. For instance [22] propose to use a so called p-approximation of the temperature profile within U-pipes. [23, 24] develop other analytical solutions taking into account interactions between the pipes. However despite the high efficiency of all these methods, they are still limited in geometry, soil configuration

and complexity of couplings.

The last decade gives birth to a large number of different numerical models of BHE. These models allow more flexibility on thermal properties distribution within the soil, modelling of an advection flow around the BHE, varying geometries, short-term description of the temperature variations... They could be classified with respect to different criteria [25]

1. numerical method: finite element (most of the following papers), finite differences [26, 27], finite volumes [25, 28];
2. 2D or 3D simulations;
3. treatment of circulating fluid transport;
4. representation of the grouting;
5. possible advection in the soil [29];
6. single or multiple borehole(s).

Fully coupled 3D models of BHE are most of the time very computationally demanding. However the continuous increase of computational power allows their intensive use. Indeed, many case studies are inherently 3D, especially when multiple boreholes are involved, the soil is heterogeneous or in case of waterflow in the ground.

Advection of heat within the pipe and diffusion within the soil are two phenomena with distinct time constant and numerical requirements (time step or mesh limitations). A pioneering work of [30] and [31] early distinguishes the BHE from the soil finite elements. In this model, the BHE (including one or two U-pipes and the grouting) is modelled as a 1D finite element. This was extended to higher number of pipes in the grouting [32, 33] or to multiple dof representing the grouting [34]. This decomposition of the pipes and the volume element becomes classical in the modelling of BHE. Another model describes the BHE as an assembling of resistances and thermal capacity [26, 35]. The enumeration of the different models is not the purpose of this paper but interested reader should refer to [25] as a starting point.

Many models deal with steady-state solutions for the temperature distribution within the pipe. However it appears that the dynamic modelling of BHE is a crucial issue in their design [36, 37, 38]. [39] conclude that alternative and discontinuous operation modes can strongly increase the heat transfer efficiency. Heat pump are often used in alternative modes and periods ranging from a year to less than a day. In the first case, heat extraction (winter) and injection (summer) modes alternate over a year [40, 25]. In the second case, the heat pump may work only for a part of the day and be switched off otherwise [41, 19]. Subsequently there is a need of a model able to reproduce highly transient effects with a minimum error and computer cost. Indeed, the error accumulation may be a critical issue [42] in case of cycle thermal loading.

The objective of the paper is to present the formulation of a versatile finite element of heat exchanger. The classical basic idea consists in dissociating the advective problem within the pipes and the dispersive problem within the grouting and the soil. The focus is placed here not on the large-scale modelling of

multiple BHE but on the accurate modelling of a single BHE in the near and far fields. The grouting around the pipes is then explicitly modelled in order to well reproduce the gradients of temperature inside it and to avoid any hypothesis on the grouting thermal resistance or the interaction between different pipes. The geometry of the grouting section may also evolves with depth due to the heterogeneity of the soil. The model must accurately reproduce long and short term variations of temperature around the borehole.

The finite element is implemented in the non-linear finite element code LAGAMINE developed at the University of Liege [43, 44]. This software is able to take into account all thermo-hydro-mechanical couplings in a fully coupled manner. However only thermal effects are considered here. The formulation of the element is adapted to highly transient simulations. Moreover the error control is a major concern. Indeed, the integration scheme and parameters are of crucial importance for advection problem.

In the following, the coupled heat exchanger finite element is firstly described in a general manner. It is validated on a classical example and verified with respect to a line source analytical solution. Numerical examples are then presented. A short-term heat injection scenario is investigated to prove the capabilities of the model and to estimate the error due to time integration parameter. A short-period discontinuous heat extraction scenario is presented and the influence of the operation scheme is analysed. Finally a one year simulation is carried out taking into account daily variations of the thermal demand.

2. Heat exchanger finite element

In the following it is decided to represent the pipe inside the BHE as a 1D finite element. Contrary to many models, the 1D finite element only models the flow into the pipes and does not include the grouting. This allows a very flexible formulation where the number, the disposition and the interaction of the pipes inside the borehole is arbitrary. The fluid flow is supposed to be in steady-state and the fluid velocity is constant all along the pipes.

Each node of the pipe element is related to a node, representative of the surrounding ground temperature. Here the ground is a generic denomination of the volume surrounding the pipe irrespectively of its actual nature (grouting, soil...). The volume 8-node finite elements describing the ground are classical and defined in [45] for thermo-hydro-mechanical couplings. They take into account thermal conduction into the soil and could also deal with advection, despite this is not considered in the following.

2.1. Governing equations

Let us assume a pipe is embedded into a ground volume of arbitrary shape, as depicted in Figure 1. A fluid is circulating within the pipe and there is a difference of temperature between the fluid and the surrounding ground. It is assumed that the cross-section of the pipe is constant all over the pipe. Moreover the temperature of the fluid is assumed uniform over each cross-section and the

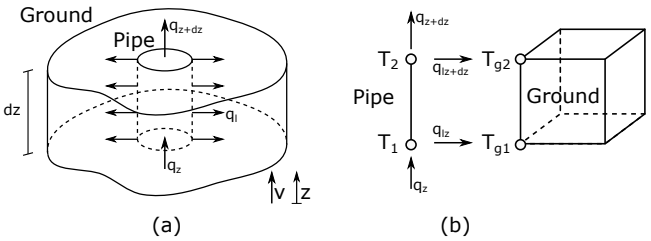

Figure 1: (a) Sketch of the control volume, (b) idealisation of the problem

velocity of the fluid is constant all along the pipe. The incoming longitudinal heat flux q_z [W/m^2] into the pipe is composed of a conduction and an advection terms such that

$$\mathrm{q}_z = -k\frac{\partial \mathrm{T}}{\partial z} + v\,\rho\,c_p\,(\mathrm{T} - \mathrm{T}_{ref})\,, \tag{1}$$

where k [W/m/K] is the thermal conductivity, v [m/s] is the velocity of the fluid, ρ [kg/m^3] is the mass density of the fluid, c_p [J/kg/K] is the specific heat of the fluid, T [K] is the temperature of the fluid and T_{ref} [K] is a reference temperature. The outcoming heat flux $\mathrm{q}_{z+\mathrm{d}z}$ is derived from

$$\mathrm{q}_{z+\mathrm{d}z} = \mathrm{q}_z + \frac{\partial \mathrm{q}_z}{\partial z}\,\mathrm{d}z. \tag{2}$$

It is assumed that the convective heat exchange through the lateral surface of the pipe q_l [W/m^2] depends on the difference of temperature between the temperature of the fluid and the representative temperature of the ground T_g [K], leading to

$$\mathrm{q}_l = h\,(\mathrm{T}_g - \mathrm{T})\,, \tag{3}$$

where h [W/m^2/K] is the convective heat coefficient. This coefficient rules the exchange of heat between the fluid and the wall of the pipe but may also include the thermal resistance of the pipe. Considering the control volume represented in Figure 1(a), the heat balance equation for the pipe is expressed as

$$\rho\,c_p\,S\,\mathrm{d}z\,\frac{\partial \mathrm{T}}{\partial t} = S\,(\mathrm{q}_z - \mathrm{q}_{z+\mathrm{d}z}) + h\,P\,\mathrm{d}z\,(\mathrm{T}_g - \mathrm{T}) \tag{4}$$

where P [m] is the circumference of the pipe and S [m^2] its section. Introducing Equations (1) and (2) into (4) yields to the governing equation of the heat flux within the pipe

$$\rho\,c_p\,S\,\mathrm{d}z\,\frac{\partial \mathrm{T}}{\partial t} + S\,\left(-k\frac{\partial^2 \mathrm{T}}{\partial z^2} + v\,\rho\,c_p\,\frac{\partial \mathrm{T}}{\partial z}\right)\,\mathrm{d}z - h\,P\,\mathrm{d}z\,(\mathrm{T}_g - \mathrm{T}) = 0. \tag{5}$$

2.2. Initial and boundary conditions

Initially at time $t = 0$, the temperature within the soil is set equal to the representative temperature of the ground T_g at the beginning, such that

$$\mathrm{T}(z, 0) = \mathrm{T}_g(z, 0). \tag{6}$$

Two types of boundary conditions can be imposed on surfaces normal to the axis of the pipe: essential (Dirichlet) and natural (Neumann) conditions. The first condition consists in imposing the temperature of the fluid. For instance imposing the temperature at the beginning of the pipe reads

$$\mathrm{T}_{z_{in},t} = \mathrm{T}_{in}, \tag{7}$$

where z_{in} is the position of the pipe's inlet and T_{in} the imposed temperature.

The Neumann condition imposes a heat flux on the inlet or outlet surface of the pipe. The heat flux in any cross-section is computed according to Equation (1). A first condition applied in the following consists in a "free flow", which allows the heat to go out of the pipe. In this case, the q_{out} flow is imposed on the outlet cross-section such that

$$q_{out} = -k\frac{\partial \mathrm{T}}{\partial z} + v\,\rho\,c_p\,(\mathrm{T} - \mathrm{T}_{ref})\,. \tag{8}$$

The carrier circulating fluid often describes a loop and is heated by a heat at the top of a U-pipe. In this case, the free-flow condition is applied to the outlet section and the q_{in} flow is applied at the inlet cross-section according to

$$q_{in} = -k\,\frac{\partial \mathrm{T}}{\partial z} + v\,\rho\,c_p\,(\mathrm{T} - \mathrm{T}_{ref}) + \frac{Q_p}{S}, \tag{9}$$

where Q_p [W] is a power provided to the fluid.

2.3. Weak formulation of the problem

The exact residual Equation (5) is numerically solved over an arbitrary domain by the weighted residual method [46]. The following equation holds over a 1D domain of length L

$$S\int_0^L \mathrm{W}(z)\,\rho\,c_p\,\frac{\partial \mathrm{T}}{\partial t}\,\mathrm{d}z - S\int_0^L \mathrm{W}(z)k\,\frac{\partial^2 \mathrm{T}}{\partial z^2}\,\mathrm{d}z + S\int_0^L \mathrm{W}(z)\,v\,\rho\,c_p\frac{\partial \mathrm{T}}{\partial z}\,\mathrm{d}z - P\int_0^L \mathrm{W}(z)\,h\,(\mathrm{T}_g - \mathrm{T})\,\mathrm{d}z = 0 \tag{10}$$

where $W(z)$ is an arbitrary weighting function. Equation (10) is integrated by parts and the resulting weak formulation of the problem is then provided by,

$$S\int_0^L \mathrm{W}(z)\,\rho\,c_p\,\frac{\partial \mathrm{T}}{\partial t}\,\mathrm{d}z - S\int_0^L k\,\frac{\partial \mathrm{W}(z)}{\partial z}\,\frac{\partial \mathrm{T}}{\partial z}\,\mathrm{d}z + S\int_0^L \mathrm{W}(z)\,v\,\rho\,c_p\,\frac{\partial \mathrm{T}}{\partial z}\,\mathrm{d}z - P\int_0^L \mathrm{W}(z)\,h\,(\mathrm{T}_g - \mathrm{T})\,\mathrm{d}z = \left[k\,W(z)\,\frac{\partial \mathrm{T}}{\partial z}\right]_0^L, \tag{11}$$

where the right-hand term is a boundary condition term.

2.4. Space discretisation of the problem

The field of temperature in the pipe is discretised by two-node isoparametric finite elements as described in Figure 1. A mapping described by the Jacobian matrix **J** rules the change of variable from global coordinates (x,y,z) to local coordinate (ξ). Therefore the continuous field of temperature T is described over an element by

$$\mathrm{T}(\xi) = \mathbf{N}^T \, \tilde{\mathbf{T}}, \tag{12}$$

where $\tilde{\mathbf{T}}^T = \left[\tilde{\mathrm{T}}_1, \tilde{\mathrm{T}}_2\right]$ is the vector of nodal temperatures and $\mathbf{N}^T = [\mathrm{N}_1(\xi), \mathrm{N}_2(\xi)]$ is the vector of shape functions related to these nodes. They are defined according to

$$\mathrm{N}_1(\xi) = \frac{1}{2}\,(1-\xi)\,, \tag{13}$$

$$\mathrm{N}_2(\xi) = \frac{1}{2}\,(1+\xi)\,. \tag{14}$$

The field of representative ground temperature parallel to the pipe is described similarly,

$$\mathrm{T}_g(\xi) = \mathbf{N}^T \, \tilde{\mathbf{T}}_g, \tag{15}$$

but the shape functions are related to nodes of the ground $\mathbf{T}_g = [\mathrm{T}_{g1}, \quad \mathrm{T}_{g2}]^T$ in Figure 1.

Galerkin finite elements where the weighting functions are identical to the shape functions are classically used. However for advection-diffusion problems, it is shown that spurious oscillations may appear [47]. A lot of attention has been paid to this problem over the years. One solution is to use Petrov-Galerkin weighting functions [48, 49]. Such a solution is already adopted for BHE in [30, 32]. The weighting functions related to the pipe nodes are gathered into the vector $\mathbf{W}^T = [\mathrm{W}_1(\xi), \mathrm{W}_2(\xi)]$,

$$\mathrm{W}_1(\xi) = \frac{1}{2}\,(1-\xi) - \frac{3}{4}\,\beta\,\left(1-\xi^2\right) \tag{16}$$

$$\mathrm{W}_2(\xi) = \frac{1}{2}\,(1+\xi) + \frac{3}{4}\,\beta\,\left(1-\xi^2\right), \tag{17}$$

where β is a parameter depending on the Peclet number Pe such that

$$\beta = \coth\left(Pe\right) - \frac{1}{Pe}, \tag{18}$$

and the Peclet is defined according to

$$Pe = \frac{v\,\Delta z}{k}, \tag{19}$$

where Δz is the length of the 1D finite element. The weighting functions are represented in Figure 2 for different values of β. This represents the functions related to a node centred in $\xi = 1$ for two adjacent elements. The speed of the

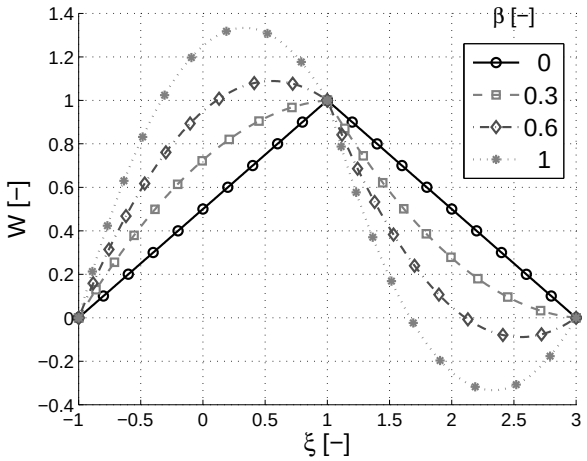

Figure 2: Petrov-Galerkin weighting functions

flow is oriented towards positive axis. These functions simply give more weight to information coming from the direction of the flow.

Injecting Equations (16)-(17) into Equation (11) leads after some algebra (dropping boundary terms $\tilde{\mathbf{W}}$) to a residual equation

$$\mathbf{F}_p^e = S \int_{-1}^{1} \rho\, c_p\, \mathbf{W}\, \frac{\partial \mathrm{T}}{\partial t}\, |\mathrm{J}|\, \mathrm{d}z - S \int_{-1}^{1} k\, \left[\frac{\partial \mathbf{W}}{\partial z}\right]\, \frac{\partial \mathrm{T}}{\partial z}\, |\mathrm{J}|\, \mathrm{d}z + S \int_{-1}^{1} \mathbf{W} v\, \rho\, c_p\, \frac{\partial \mathrm{T}}{\partial z}\, |\mathrm{J}|\, \mathrm{d}z$$
$$-P \int_{-1}^{1} \mathbf{W}\, h\, (\mathrm{T}_g - \mathrm{T})\, |\mathrm{J}|\, \mathrm{d}z \tag{20}$$

where |J| is the determinant of the Jacobian matrix $\mathbf{J}$, equal to $L/2$. Vector $\mathbf{F}_p^e$ is also termed vector of energetically equivalent nodal forces. It is an elementary vector related only to nodes of the pipe. The solution is in equilibrium if $\|\mathbf{F}_p^e\| = 0$. Otherwise, there are out of balance forces that should be reduced. This formulation is general and remains valid even if thermal properties varies with temperature. This vector is defined individually for each finite element.

The lateral heat flux Equation (3) consists of a source term for the ground domain around the pipe. Therefore energetically equivalent nodal forces on the ground side, $\mathbf{F}_g^e$, are defined similarly such that

$$\mathbf{F}_g^e = P \int_{-1}^{1} \mathbf{N}^T\, h\, (\mathrm{T}_g - \mathrm{T})\, |\mathrm{J}|\, \mathrm{d}z. \tag{21}$$

Only the heat exchange between the pipe and the ground is taken into account. In this case, the weighting functions are identical to the shape ones in order to

be consistent with the ground finite elements [30, 31].
Equations (20) and (21) are defined at the level of a single element. The last step is the assembling of a global vector of energetically equivalent nodal forces, **F**. This step is somehow classical and not detailed here.

2.5. Resolution of the problem

The time continuum is discretised in different time steps of duration Δt_n such that

$$t_{n+1} = t_n + \Delta t_n. \tag{22}$$

The duration of the time steps may evolve during the simulation. It is supposed that the nodal unknowns vary linearly over a time step such that

$$\tilde{\mathbf{T}}_{n+\theta} = (1-\theta)\,\tilde{\mathbf{T}}_n + \theta\,\tilde{\mathbf{T}}_{n+1} \qquad \theta \in [0,1]. \tag{23}$$

Therefore the out of balance nodal forces can be computed for any θ. Solving the problem consists in finding the final nodal temperature vector $\tilde{\mathbf{T}}_{n+1}$ at the end of the time steps ensuring the out of balance forces $\mathbf{F}_{n+\theta}\left(\mathrm{T}_{n+\theta}\right)$ are equal to zero. If the θ parameter is equal to 0, the integration is explicit. Otherwise the resolution is implicit. The fully implicit scheme corresponds to $\theta = 1$ and $\theta = 0.5$ is the so called Crank-Nicholson scheme.
If the problem is linear and the time step constant the elementary stiffness matrix $\mathbf{K}^k$ is unique and comes from

$$\mathbf{K} = \frac{\partial \mathbf{F}_{n+\theta}}{\partial \tilde{\mathbf{T}}_{n+1}} = \frac{\partial \mathbf{F}_{n+\theta}}{\partial \tilde{\mathbf{T}}_{n+\theta}} \frac{\partial \tilde{\mathbf{T}}_{n+\theta}}{\partial \tilde{\mathbf{T}}_{n+1}} = \theta\,\frac{\partial \mathbf{F}_{n+\theta}}{\partial \tilde{\mathbf{T}}_{n+\theta}}. \tag{24}$$

Finally, the heat storage is considered as a component of the out of balance forces. It is assumed that $\partial \mathbf{T}/\partial t$ is constant over the time step and

$$\left.\frac{\partial \tilde{\mathbf{T}}}{\partial t}\right|_{n+\theta} = \frac{\tilde{\mathbf{T}}_{n+\theta} - \tilde{\mathbf{T}}_n}{\theta\,\Delta t}. \tag{25}$$

The expression of the elementary stiffness matrix related to nodal unknowns $\left[\tilde{\mathrm{T}}_1, \tilde{\mathrm{T}}_2, \tilde{\mathrm{T}}_{g1}, \tilde{\mathrm{T}}_{g2},\right]^T$ is then summarised into the expression,

$$\mathbf{K}^e = \begin{bmatrix} \mathbf{K}_{pp} & \mathbf{K}_{pg} \\ \mathbf{K}_{gp} & \mathbf{K}_{gg} \end{bmatrix}, \tag{26}$$

where the p subscript corresponds to the pipe and g to the ground. For instance the definition of the pipe-pipe component reads

$$\mathbf{K}_{pp} = \frac{S}{\theta\,\Delta t} \int_{-1}^{1} \mathbf{W}\,\rho\,c_p\,\cdot \mathbf{N}^T\ |\mathrm{J}|\ \mathrm{d}z - S \int_{-1}^{1} k\,\frac{\partial \mathbf{W}}{\partial z} \cdot \left[\frac{\partial \mathbf{N}}{\partial z}\right]^T |\mathrm{J}|\ \mathrm{d}z + S \int_{-1}^{1} v\,\rho\,c_p\,\mathbf{W} \cdot \left[\frac{\partial \mathbf{N}}{\partial z}\right]^T |\mathrm{J}|\ \mathrm{d}z$$
$$+P \int_{-1}^{1} h\,\mathbf{W} \cdot \mathbf{N}^T\ |\mathrm{J}|\ \mathrm{d}z \tag{27}$$

The explicit definition of all components is provided in Appendix B for temperature independent thermal properties. Finally all the elementary stiffness matrices are assembled to the global stiffness matrix that will be solved.

3. Validation of the finite element

In the following section, the developed finite element is validated with respect to analytical solutions. A simplified geometry is considered in order to stay as close as possible to the hypotheses of the analytical solution.

3.1. Problem investigated

The geometry of the problem is illustrated in Figure 3. The geometry consists of a single pipe coupled to a sector (opening of 10°) of ground. This ground represents a unique material whose properties are given in Table 1. The validity of the coupling with a 3D domain is shown but the computational time is limited. The external radius of the sector (ground domain) is equal to 6m and its depth to 40m. The mesh is laterally refined near the centre and more spaced further. It is uniformly discretised over the depth ($\Delta z = 1$m). The carrier circulating fluid is supposed to be pure water.
The top boundary of the pipe condition consists of an imposed temperature or an imposed flux. The bottom condition is either an open pipe (the fluid goes away) or a loop condition (the fluid is heated and injected back to the top). This latter condition is non-realistic since the fluid is instantaneously transported. However this condition better suits the analytical line source solution, namely there is a single pipe. The ground domain is supposed to be in adiabatic conditions. The temperature is recorded in the pipe and in a cross-section at mid-depth as depicted in Figure 3.
The rigorous choice of a time step to solve a transient problem depends on physical and numerical parameters. It is known that there is a critical time step that should not be overpassed in order to ensure the stability of the simulation, especially if the solution scheme is explicit. This conditions for convection dominated 1D problems is summarised into the Courant number condition [50, 47],

$$\frac{v\,\Delta t}{\Delta z} \leq 1. \tag{28}$$

This involves that the time step between two successive computations of a solution must be less than the time required for the perturbation to travel across the length of a finite element. The maximum time step of the simulation is equal to 3s in order to fulfil the Courant requirement such that

$$\frac{v\,\Delta t}{\Delta z} = 0.9 \leq 1. \tag{29}$$

The convective heat transfert coefficient h is calculated according to

$$h = \frac{Nu\,k_w}{D_h}, \tag{30}$$

	1D Pipe	Ground
ρ [kg/m^3]	1000	2500
c_p [kJ/kg/K]	4.185	0.92
k [W/m/K]	0.58	2.94
v [m/s]	0.3	/
r [m]	0.0131	/
μ [N.s/m^2]	1.002E-3	/
h [W/m^2/K]	1500	

Table 1: Material parameters of the sector problem

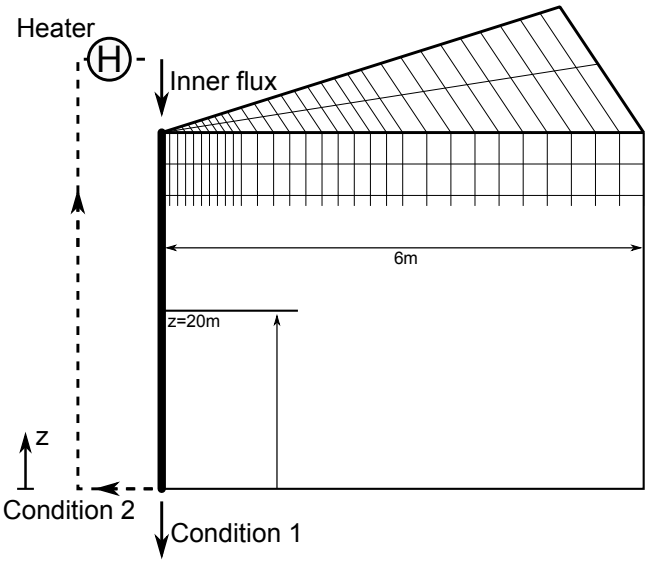

Figure 3: Sketch of the mesh and parameters for the validation of coupled finite elements

where D_h [m] is the hydraulic diameter of the pipe ($= 2r$), k_w [W/m/K] the fluid thermal conductivity and Nu [-] the Nusselt number obtained from the classical correlation [51],

$$Nu = \frac{(f/8)\ (Re - 1000)\ Pr}{1 + 12.7\,(f/8)^{1/2}\ \left(Pr^{2/3} - 1\right)}, \qquad 0.5 < Pr < 200, \quad 3000 > Re > 5\,10^6. \tag{31}$$

This relation depends on the Reynolds number Re [-],

$$Re = \frac{\rho\, v\, D_h}{\mu}, \tag{32}$$

where ρ [kg/m^3] is the density of the fluid, v [m/s] the average velocity and μ [Pa.s] is the dynamic viscosity. The Prandtl number Pr [-] is defined as

$$Pr = \frac{c_p\, \mu}{k} \tag{33}$$

where c_p [J/kg/K] is the specific heat. Finally the Darcy friction factor f [-] is computed according to

$$f = (0.79 \ln(Re) - 1.64)^{-2} \tag{34}$$

for smooth pipes. The final convective heat transfer coefficient h computed is equal to 1500 W/m/K. It is related to parameters provided in Table 1 for the 1D pipe.

3.2. Constant soil temperature

The steady-state solution of the advection-diffusion problem in the pipe is easily obtained if the soil is assumed to have a constant temperature. The analytical solution of the temperature profile in the pipe is provided by [52]

$$\mathrm{T}(z) = \mathrm{T}_g - (\mathrm{T}_g - \mathrm{T}_i) \exp\left(\frac{-2\pi\, r\, z}{\pi\, r^2\, v\, \rho\, c_p}\, h\right) \tag{35}$$

where T_i [K] is the imposed temperature at the beginning of the pipe. A numerical simulation is run where the initial inlet temperature is instantaneously heated from the initial temperature of 285K to 300K. Numerically there is a first short transient phase where the perturbation propagates inside the pipe. The vertical distributions of temperature along the pipe at different time steps are provided in Figure 4.
For the first time step, there is a small non-physical oscillation located around z= 35m after 10s. This is simply due to a mesh too coarse to exactly reproduce a very steep propagation front. After more than 90s, the numerically computed distribution of temperature in the pipe perfectly matches the analytical steady-state solution.

3.3. Variable soil temperature

In the following, a heating test is simulated. It is assumed that the fluid going out of the pipe (z=0m) is instantaneously injected at its beginning (z=40m) and heated by a power Q_p of 2kW. This leads to an average heating flux of the BHE q_{av} equal to 50W/m. The evolution of the temperature in three sections of the pipe is provided in Figure 5. The log scale is chosen to distinguish between transient and stationary phases. Temperature is constant until the incoming heated fluid reaches the observation point. Temperature is continuously increasing afterwards since the fluid describes a loop.

The distribution of temperature within the pipe at different time steps is provided in Figure 6. Results on the left of the figure depicts the transient phase of the temperature evolution. The temperature profile is curved and temperature is higher at the top of the pipe. After few hours, the temperature profile has a constant shape that is simply shifted. This is a kind of stationary phase despite the evolution of temperature is still ongoing.

The evolution of convective fluxes corresponding to Equation (3) in the three cross-sections is depicted in Figure 7. They are quite different during the first

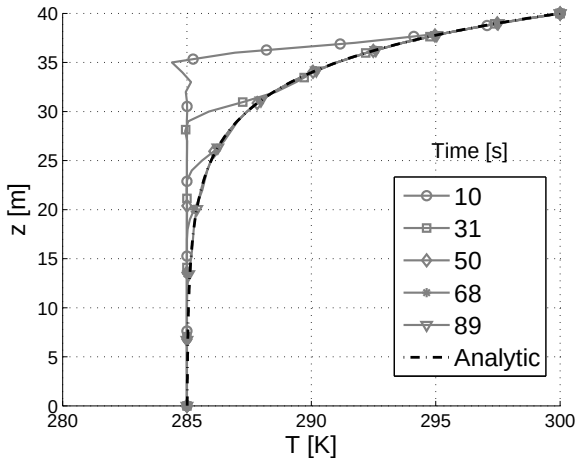

Figure 4: Distribution of the temperature in the pipe at difference time steps, constant soil temperature

hour but almost converge towards the average value at the end. At the beginning the heat flux is the highest near the inlet of the pipe where the fluid has the highest temperature. Consequently the ground is heated, which progressively decreases the heat flux. Indeed the difference of temperature between the fluid and the ground is reduced. This highly transient phase is roughly limited to less than an hour. Afterwards the heat flux stabilises.

The line source model is frequently used to validate results of transient simulations of heat exchanger [31]. It consists of the heating of a semi-infinite medium where the heating fluxes are normal to a vertical line. The initial temperature in the ground and the pipe is uniform at the beginning. The radial distribution of temperature within the soil follows

$$\mathrm{T} = \mathrm{T}_{g0} + \frac{q}{2\pi\, k} \int_{\epsilon}^{\infty} \frac{\exp(-\xi^2)}{\xi}\, \mathrm{d}\xi, \tag{36}$$

$$\epsilon = \frac{r}{2\sqrt{\alpha\, t}}, \tag{37}$$

where T_{g0} [K] is the initial temperature of the ground, q [W/m] is the average heat flux per meter length of the borehole, r [m] the radial distance to the source $\alpha = k/\rho/c_p$ [s^{-1}] is the thermal diffusivity of the soil and t [s] the time. An analytical solution of the integrand of Equation (36) is provided if $\epsilon < 0.2$ [53],

$$I(\epsilon) = \ln\frac{1}{\epsilon} + \frac{\epsilon^2}{2} - \frac{\epsilon^4}{8} - 0.2886. \tag{38}$$

The accuracy of that solution is then a function of position and time. The correct solution for a point lying far from the heating source is only available for a long time operation.

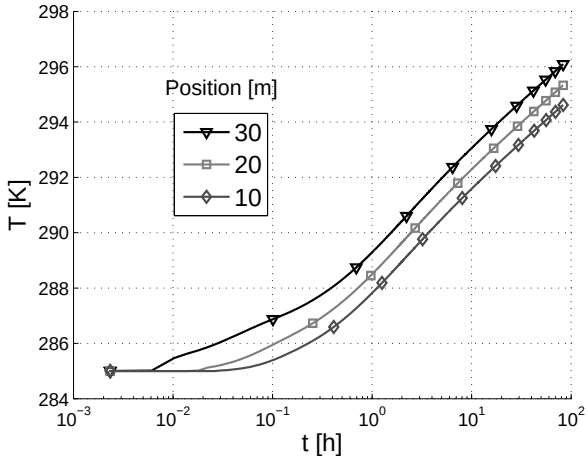

Figure 5: Time evolution of the temperature in the pipe at three vertical positions

The mid-depth section is the point where the lateral heat flux is the closest from the average value. Therefore the horizontal temperature profile in the ground at this depth is compared with the line source solution in Figure 8. Three time steps are investigated. Numerical and analytical solutions present a very good agreement. They slightly diverge but this could be explained by the non-constant heat flux over the depth and time, the mesh discretisation at the centre of the sector and vertical diffusion.

According to the line-source model, the conductivity of the soil can be estimated according to [52, 27]

$$k_{est} = \frac{q}{4\,\pi}\,\frac{\log(t_{n+1}) - \log(t_n)}{\mathrm{T}_{n+1} - \mathrm{T}_n}. \tag{39}$$

The time-evolution of this estimated conductivity computed using the evolution of fluid temperature at three depths is provided in Figure 9. The estimated value at the beginning of the simulation has no meaning since it lies in the highly transient phase where the heat fluxes are not stabilised. Moreover this phase is mainly controlled by the grouting properties. Finally the back-calculated values tend to the imposed values.

4. Numerical examples

In this section, the capabilities of the model are described by different examples. A real case study is investigated where a U-pipe of 100m is modelled. Short- and long-term simulations are presented. The 3D simulations are cpu time consuming. Therefore the time steps of the simulations are frequently chosen much higher than what is required by the Courant condition for advection-diffusion problems. The influence of the maximum time step of the simulation

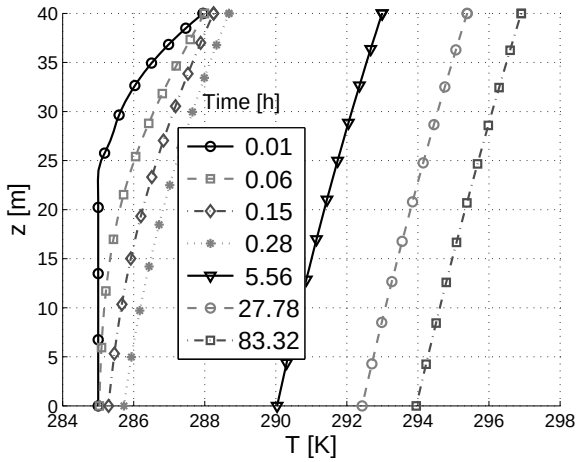

Figure 6: Distribution of the temperature in the pipe at difference time steps

on the error is investigated. A cyclic example combining transient and long term phenomena is also presented. Finally a one year simulation exhibits differences in results due to daily or annual variations of thermal demand.

4.1. Problem investigated

The geometry consists of a single U-tube embedded in a borehole of radius equal to 6.8 cm as shown in Figure 10. Both pipes of radius equal to 1.31cm are separated by 6.8 cm. The grouting is explicitly modelled.
The 1D finite element of pipe that is used does not occupy any volume, by definition. However the pipe are physically embedded in the grouting and fill a volume. [54] propose to use a pseudo-pipe material to discretise this volume. This method is adopted here as shown in Figure 10. This material has a high conductivity in order to not introduce an additional thermal resistance. However contrary to [54] there is no heat capacity assigned to the material to avoid the introduction a spurious transient phase within the pipe cross-section where temperature is supposed to be constant.
The 1D pipe element is connected to the central node the pseudo-pipe's volume. The pipe material is not represented here but the geothermal resistance could be included in the convective heat transfer coefficient h. The different material parameters are provided in Table 2. The vertical direction is discretised in 105 slices with a height of 1m. The total size of the mesh is equal to almost 95000 unknowns. The simulations are run in adiabatic conditions and the initial temperature is uniform and equal to 285K.

4.2. Heating simulation

The first simulation consists of a thermal response test during 50000s (13.89h). The time step is equal to 3s. The fluid describes a loop and is heated continu-

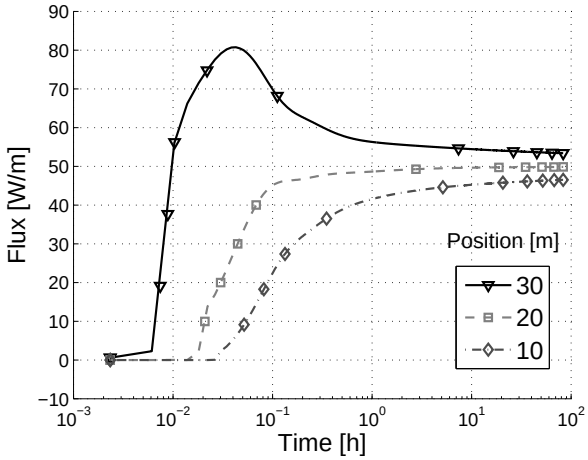

Figure 7: Time evolution of the pipe-soil heat convective flux at three vertical depths

	1D Pipe	Pseudo-pipe	Grouting	Soil
$\rho\, c_p$ [MJ/^{3}/K]	4.18	0	1.62	2.3
k [W/m/K]	0.58	200	2.35	2.94

Table 2: Material parameters of the U-pipe problem

ously. Temperature profiles within the pipe are provided in Figure 11 in order to describe the behaviour of the installation. The observed distribution of temperature quickly reaches its steady state where a similar V shape profile is progressively translated towards higher temperatures.

Different cross-sections of the grouting and the pseudo pipes at the end of the heating are depicted in Figure 12. Temperature over the pseudo-pipe material is almost constant which was intended. On the contrary, temperature distribution in the grouting is everything but uniform.

The highest gradients of temperature within the grouting are observed in z=100m, which is the section closest to the pipe inlet. This is consistent with the temperature profile distribution in Figure 11 since the difference of temperature is the highest. On the contrary, the distribution of temperature is symmetric at the bottom of the borehole, where the temperature is identical in both pipes. The accurate simulation of the temperature gradient is crucial for their sustainability since the induced thermal stresses may degrade the grouting [11, 20, 12]. The mechanical degradation of the grouting is correlated with a decrease of its thermal properties and then its efficiency.

Figure 13 exhibits the temperature distribution in the very near area around the grouting at the end of the simulation. Indeed, the distribution is non-symmetric around the borehole due to the downstream and upstream pipes. However the symmetry of the temperature profile fast becomes symmetric at a radial distance

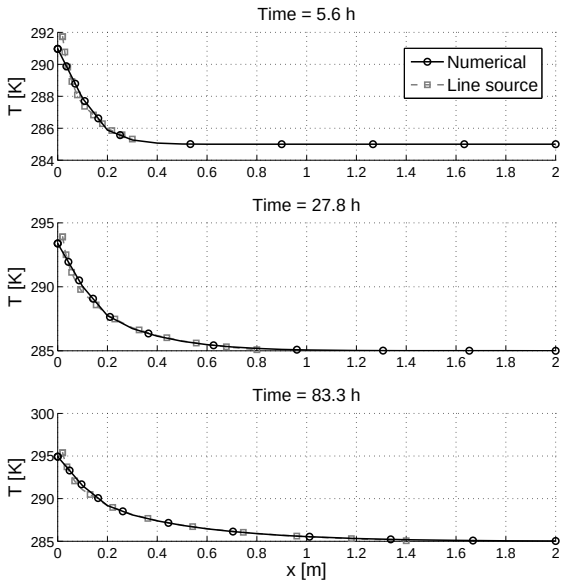

Figure 8: Distribution of the temperature in the soil at difference time steps at z= 20m, comparison between infinite line-source and numerical results

lower than 50cm. Moreover, the symmetry also increases with depth. Therefore from a practical point of view, the line source like models are sufficient to study the long-term behaviour of BHE for homogeneous soils without waterflow.

4.3. Error assessment

In many applications, the duration of the simulation ranges from days to years [31, 28, 27]. Large time steps are commonly carried out to spare cpu time and the fully implicit method is mainly adopted. However as previously mentioned in Section 3.1, the time step in advection-diffusion problems is classically limited by the Courant number. Moreover the θ parameter defined in Equation (23) is known to affect the results [55, 46]. A θ parameter equal to 0.5 limits numerical diffusion and provides a second order accuracy scheme for small time steps. However $\theta = 1$ is known to provide a better precision for large time steps [56]. Therefore it is interesting to assess the error arising from the choice of a time step and an integration scheme.

An error indicator must be found to summarise the error of the results. It is chosen to focus on the temperature distribution within the pipe. The following error deals with the variation of temperature rather than its absolute value as proposed in [39, 16]. The relative error at node i of the pipe and time t is defined according to

$$err(i,t) = \frac{\mathrm{T}_i(t) - \mathrm{T}_{ref,i}(t)}{\mathrm{T}_{ref,i}(t) - \mathrm{T}_0} \tag{40}$$

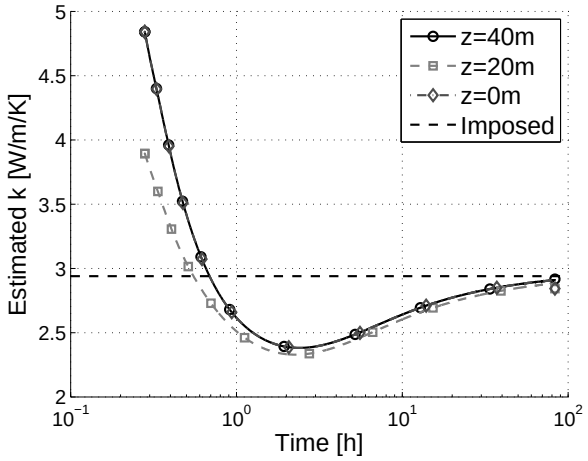

Figure 9: Time evolution of the conductivity estimated in the soil from the temperature evolution at the end of the pipe

where $T_i(t)$ [K] is the temperature of the fluid in the current simulation at node i, $T_{ref,i}(t)$ [K] is the temperature of the fluid at the same node in the reference simulation and T_0 [K] is the initial temperature. The reference simulation is the thermal response test. The reference time step is equal to 3s and the Crank-Nicholson integration scheme is adopted. The average error over the pipe at time t is defined such that

$$err_{av}(t) = \frac{1}{n_{nodes}} \sum_{i=1}^{n_{nodes}} err(i,t) \tag{41}$$

where n_{nodes} is the number of nodes of the pipe where the temperature variation is different from zero.

Simulations are carried out for three time steps ($\Delta t = 100, 1000, 5000$s) and two integration schemes: Crank Nicholson ($\theta = 0.5$) and fully implicit ($\theta = 1.0$). The evolution of the error with respect to the reference simulation is provided in Figure 14. The first 700 seconds are not provided because the error is very huge. Indeed, this corresponds to the highly transient phase and the propagation of a heat front which is not well captured but was not intended to be for larger time steps.

The error increases obviously with the size of the time step. However it can be observed that it decreases with time and is under 1% at the end of all simulations. For a given time step size, the error of the Crank-Nicholson integration is lower than the fully implicit one. However some oscillations appear for time steps equal to 1000 or 5000s. This reflects oscillations in the solution. The occurrence of oscillations has been detailed in [55] and is a consequence of the too high time step. Therefore it is decided in the following to adopt a fully implicit scheme.

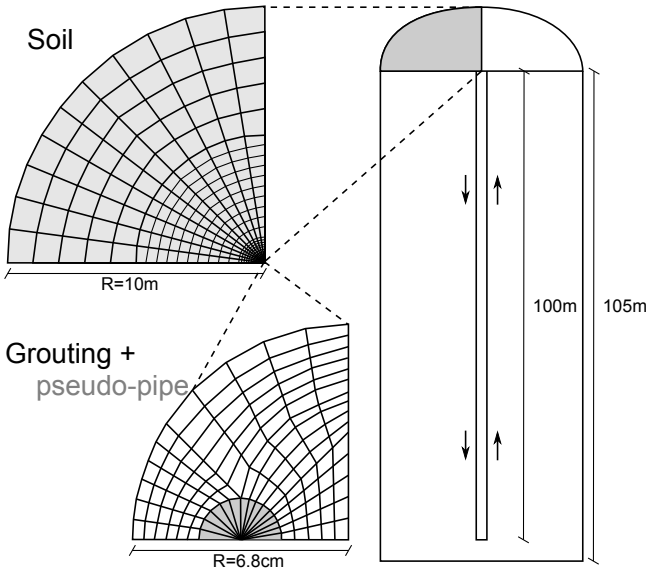

Figure 10: Sketch of the mesh of the Upipe problem

4.4. Typical thermal cyclic behaviour

The cyclic thermal loading of the borehole heat exchanger is based on the assumption that the maximum power should not necessary be maintained during a long period. For instance in office buildings or house, the human presence and use of heavy equipments is often non-continuous over a day. Therefore in the following a period of full operation ($Q_p = Q_{p,max}$,$v = v_{max}$) alternates with a period of recovery ($Q_p = 0$,$v = 0$). The duration of each period is equal to 12h. The only additional hypothesis is that the convective heat transfer coefficient h remains constant during the recovery phase even if v is equal to zero.

The evolution of the temperature in a cross-section at position z=80m is provided in Figure 15. The first cycle of heating/recovery is depicted on the left of the figure. There is a sharp cooling (starting from 285K) of the fluid followed by a slower decrease of temperature. The shape of the results is similar when the pump is switched off. However the initial temperature is not totally recovered at the end of the recovery phase which was already observed [57, 6, 58, 19]. Therefore cycle after cycle, the average temperature decreases as shown in Figure 15 on the right. This cumulated decrease of temperature is marked at the beginning but tends to slow down.

The evolution of temperature is the superposition of two distinct processes characterised by a time-scale and a zone of influence. The first is the oscillatory variation of temperature due to the alternative power. It is cyclic and has a period of 1 day. The second is the residual variation of temperature which accumulates slowly. In order to simplify the reading of the results, the time evolution signal is described by its envelope curve, that is the locus of the local

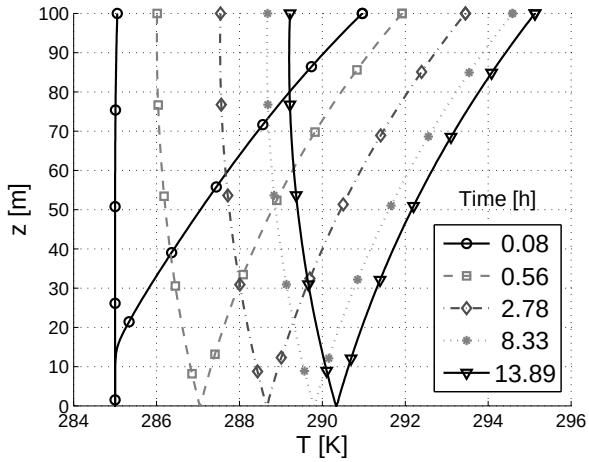

Figure 11: Distribution of temperature in the pipe of the BHE

minima or maxima, as shown in Figure 15 on the right.

Time evolution of temperature at different points of an horizontal (z=80m) cross-section are provided in Figure 16. It can be observed that the temperature cyclic amplitude is lower in the centre of the borehole (position = 0m) than in the pipe. However the trend is clearly towards freezing point. The amplitude is also smoothed with the distance from the borehole. This variation of temperature within the grouting may be a starting point for the study of its thermo-mechanical analysis.

Figure 17 presents horizontal cross sections within the soil at different depths on the downstream or upstream pipe side. In this Figure, only the last 12h of the 50th days are presented, that is only the recovery phase of the last thermal cycle is depicted. As previously mentioned, the oscillations are attenuated with distance from the borehole, depicted by the vertical dashed line. This figure clearly shows that the period of influence of the thermal cyclic loading is limited to 50cm. However the long-term influence is much larger and equal to almost 6m after 50 days.

4.5. Daily operation scheme

The following simulations investigate the influence of the daily operation scheme of the borehole heat exchanger. Three hypothetical schemes are considered in which the operating duration of the pump is respectively 8h, 12h or 16h. The pump is switched off during the remaining time of the day. The same total energy is supposed to be extracted each day, that is to say, the power is equal to 6kW, 4kW or 3kW as shown in Figure 18.

The envelope of the time evolution of the temperature at the beginning of the downstream pipe (z=100m) is provided in Figure 19. This section is the most critical since the lowest temperature of the circulating fluid is reached

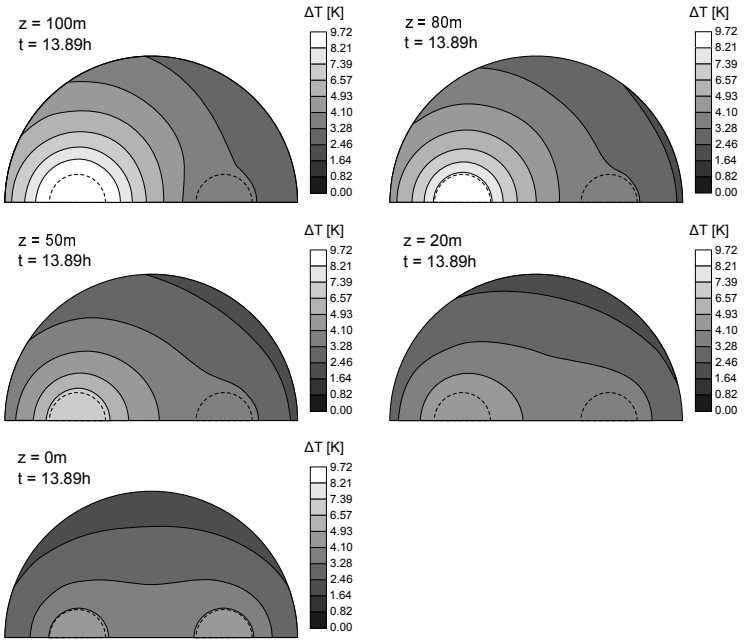

Figure 12: Cross-section within grouting and pseudo-pipes at the end of the heating (t=13.89h)

there. The tendency of the time evolution of the temperature is identical for all simulations and tends towards a decreasing temperature. However there is a clear difference between the local maxima and local minima envelopes.

The temperature recovered at the end of the off-period almost does not depend on the operating scheme. It was nevertheless observed that the dispersion increases slightly with depth. On the contrary, the lowest part of the envelope exhibits a strong dispersion. In this case, the lower the cooling power, the lower the minimum temperature. Indeed, the conduction of the soil limits the amount of heat that can be extracted from it. Therefore, for an imposed power of the pump, heat is extracted from the fluid and only partly recovered during a loop. This results has practical purpose since the lowest temperature of the fluid is limited by the freezing point of the circulating fluid. The evolution in the grouting is similar.

This result shows that the simulation of continuous heat extraction at an average cooling power is insufficient to study the sustainability of the grouting or the risk of freezing of the circulating fluid. Indeed, an average simulation would have provided an identical temperature evolution for all the previously mentioned simulations while the actual locus of minimal peaks strongly differ. These minimum values are important for the design of the BHE.

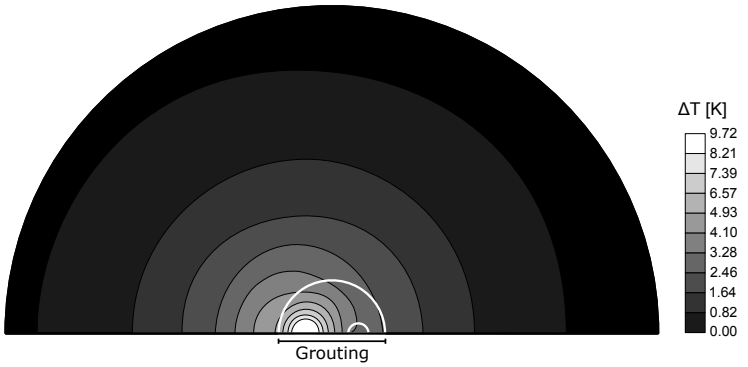

Figure 13: Cross-section within grouting, the pseudo-pipes and the soil at the end of the heating, (z=100m,t=13.89h)

A [kW]	B [kW]	C [kW]	D [kW]
-0.2	2.0	1.2	0.6

Table 3: Parameters used for the synthetic thermal load

4.6. Annual simulation

In the following, a synthetic thermal load described in [22] is used to simulation a one year operation scheme. This expression includes daily variations of the thermal demand and reads

$$Q_p(t) = A - B\,\cos\left(\frac{t}{8760}\,2\pi\right) - C\,\cos\left(\frac{t}{24}\,2\pi\right) - D\,\cos\left(\frac{t}{24}\,2\pi\right)\,\left(\frac{2\,t}{8760}\,2\pi\right), \tag{42}$$

where A [W] controls the annual load unbalance, B [W] is the half amplitude of the annual load variation, C and D [W] rule the half amplitude of the daily variations and t [d] is the time starting at mid-winter. The ratio C/D controls the damping of daily amplitude at mid-season with respect to winter or summer. Parameters used in this simulation are provided in Table 3 and the full thermal signal is depicted in Figure 20. A second thermal load profile is considered. It does not take into account the daily variations but only the annual one, as shown in Figure 20. It describes the annual trend of the full load signal.
The annual power demand evolves from negative power (heat extraction) to positive power (heat injection) but there is no exact compensation between heat extraction and injection as shown by the annual trend curve in Figure 20. The power amplitude variation is also set up higher in winter and in summer than at mid-seasons. The time step of the daily simulation is set to 2h in order to well capture the variations. On the contrary the time step of the annual simulation is set up to one day.

Figure 21 depicts the time evolution of the temperature at the inlet of the pipe. The trend of the daily simulation is well represented by the annual one.

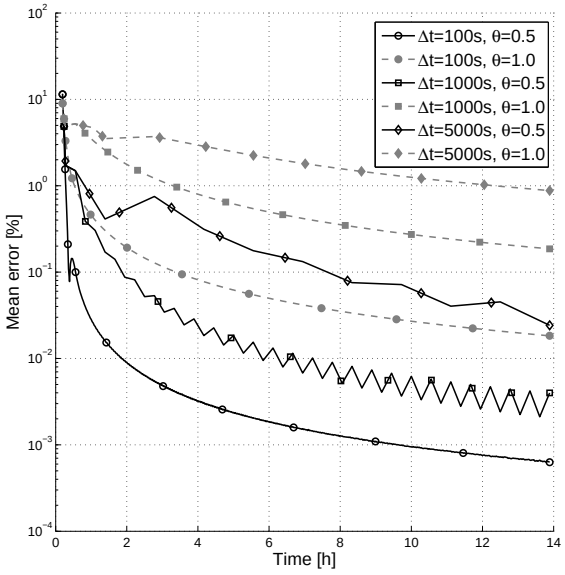

Figure 14: Mean error as a function of the time step Δt and the integration parameter θ

However the amplitude of variations may be not negligible around this trend. They are equal to almost 4K at peak. Therefore if the thermal behaviour of the circulating carrier fluid should be investigated, using only an average thermal load misses the lower/upper bound of the fluid temperature.

The daily variations of temperature are also illustrated in the centre of the borehole, as shown in Figure 22 at a depth of 80m. The amplitude of variations is lower than in the pipe. However temperature also oscillates between lower and upper bounds which could influence the thermo-mechanical behaviour of the grouting.

On the contrary, daily variations in the soil are much more damped. They almost disappear after 50cm from the centre of the borehole which was already mentioned in a previous section. Therefore if only the long term behaviour of the soil must be investigated, only the annual load signal can be used. The main advantage is the higher time step that can be used since it has been shown that the error remains negligible. Therefore the total cpu time is considerably decreased.

5. Conclusion

The aim of this paper is to formulate a finite element of heat exchanger in order to accurately model the behaviour of borehole heat exchangers. The element developed must be as flexible as possible and must reproduce transient

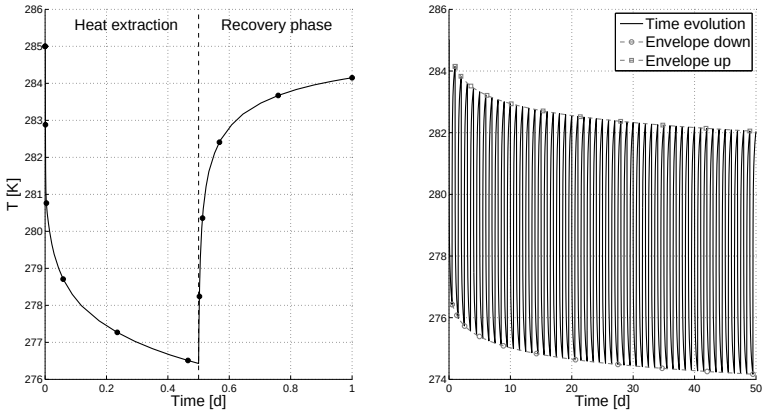

Figure 15: Time evolution of the temperature (z=80m)

and steady-state phases, near and far field distributions of temperature, and short- and long-term solutions. The focus is placed on the accurate modelling of a single BHE rather than the ability to optimise a field of BHE.

The finite element is developed in the framework of the non-linear finite element code LAGAMINE for multiphysical couplings. The advection-diffusion problem in the pipe is simplified into a 1D problem. Assuming the temperature is uniform in each cross-section, a convective exchange between the fluid inside the pipe and a temperature representative of the ground around the pipe is modelled. The weighted residual method with Petrov-Galerkin functions is adopted to solve the problem and avoid spurious oscillations. The analytical formulation of elementary out of balance force vector and stiffness matrix are provided.

The element formulation is validated by comparison with analytical solutions. Transient distributions of temperature are compared to a steady-state solution in a simplified problem where the ground temperature is fixed. Furthermore, the field of temperature within the ground is compared with the infinite line source model. Finally the back-calculation of the conductivity of the ground is carried out and compared with the imposed one.

A realistic case study is finally investigated. It consists of a single U-pipe embedded in a 100m depth borehole. Firstly a 50000s heating simulation is carried out in order to highlight the capabilities of the model. The V-shape steady-state of the temperature distribution is fast reached. Temperature distributions in cross-sections of the grouting are shown to be non-uniform over the main part of the borehole. The highest gradients of temperature are particularly visible at its top. Therefore an explicit modelling of the grouting is necessary if its thermo-mechanical behaviour is investigated. This is particularly important when there is a risk of freeze-thaw damaging. For instance this is particularly important for energy piles.

The choice of the time step and the time integration scheme on the error is

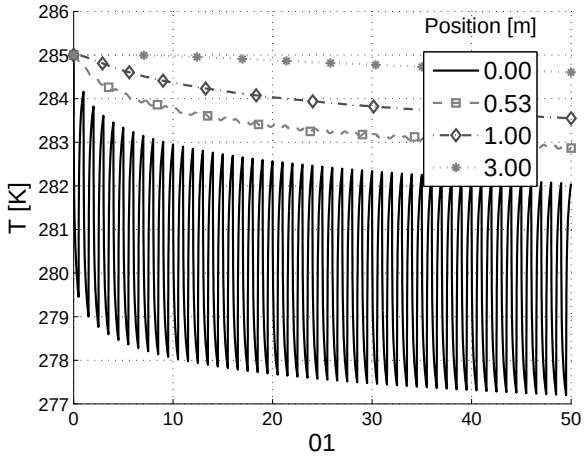

Figure 16: Time evolution of the temperature in the soil (z=80m) at different radial positions x

further investigated. It is shown that the Crank-Nicholson integration scheme leads to the lowest error for a given time step. However oscillations are likely to appear if the time step is chosen too high. On the contrary a fully implicit scheme avoids the generation of oscillations. Whatever the time step, the error is proven to decrease progressively and finally reach less than 1 percent.

The simulation of an alternating operation scheme is simulated afterwards. A period of full operation of the BHE (heat extraction) is systematically followed by a recovery period where the pump is switched off. Results exhibit the superposition of a short-term recoverable variation of temperature on a decreasing trend of the temperature within the pipe, the grouting and the soil. The influence of the cycles is limited to 50cm around the centre of the borehole while the long-term influence reaches 6m after 50days of simulation.

The influence of the operation scheme on the results is considered. An identical amount of energy is extracted over a varying operating period (8h/12h/16h) while the recovery period is equal to 16h/12h/8h. It is shown that the temperature at the end of the recovery period is almost identical. However the minimum temperature at the end of the heat extraction much more varies. If the operation period is equal to 8h, the fluid temperature decreases down to almost 270K while it remains over 276K if this period is equal to 16h.

A final one-year simulation considering both annual and daily variations in the power demand is finally run. It is shown that the annual variation of the power is sufficient to study the long term and far-field evolution of temperature within the soil. However hourly simulations with daily variations of the power are necessary if the thermo-mechanical behaviour of the grouting must be investigated. Indeed, these variations may lead to non negligible oscillations of the temperature around its trend.

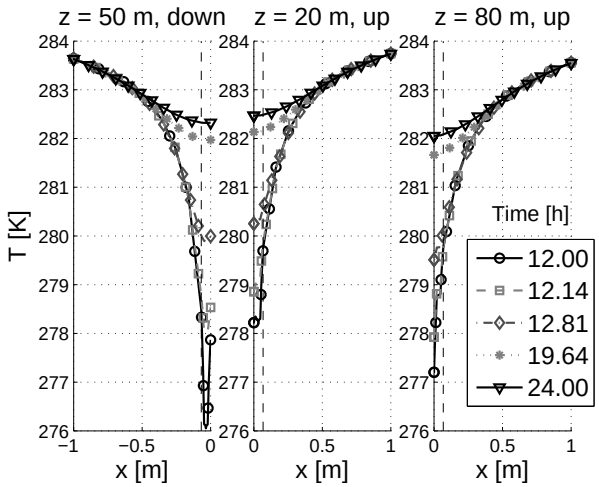

Figure 17: Distribution of temperature in the soil at different depths, recovery phase of the 50th day

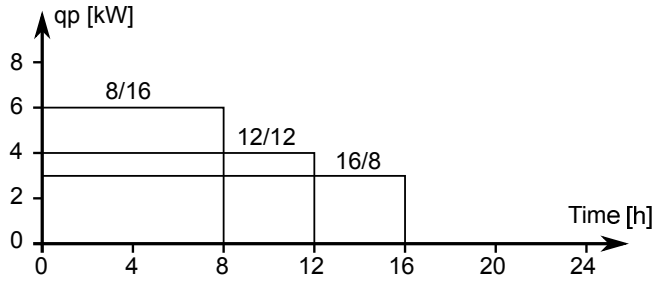

Figure 18: Daily operation schemes: operation/recovery duration

Acknowledgements

The authors would like to express their gratitude to the Walloon Region for the financial support of the project GEOTHERWAL dedicated to this topic.

References

[1] J. Lund, D. Freeston, T. Boyd, Direct utilization of geothermal energy 2010 worldwide review, Geothermics 40 (3) (2011) 159–180. doi:10.1016/j.geothermics.2011.07.004.

[2] G. Florides, S. Kalogirou, Ground heat exchangers - A review of systems, models and applications, Renewable Energy 32 (15) (2007) 2461–2478. doi:10.1016/j.renene.2006.12.014.

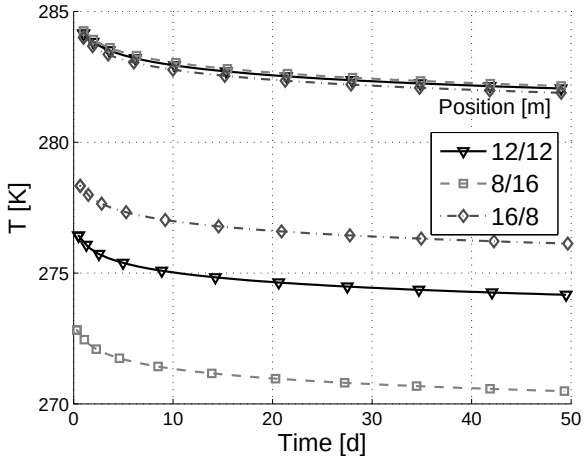

Figure 19: Envelope curves of the time evolution of the temperature in the pipe (z=80m)

[3] H. Yang, P. Cui, Z. Fang, Vertical-borehole ground-coupled heat pumps: A review of models and systems, Applied Energy 87 (1) (2010) 16–27. doi:10.1016/j.apenergy.2009.04.038.

[4] P. Bayer, D. Saner, S. Bolay, L. Rybach, P. Blum, Greenhouse gas emission savings of ground source heat pump systems in Europe: A review, Renewable and Sustainable Energy Reviews 16 (2) (2012) 1256–1267. doi:10.1016/j.rser.2011.09.027.

[5] S. Hähnlein, P. Bayer, G. Ferguson, P. Blum, Sustainability and policy for the thermal use of shallow geothermal energy, Energy Policy 59 (2013) 914–925. doi:10.1016/j.enpol.2013.04.040.

[6] L. Rybach, W. Eugster, Sustainability aspects of geothermal heat pump operation, with experience from Switzerland, Geothermics 39 (4) (2010) 365–369. doi:10.1016/j.geothermics.2010.08.002.

[7] M. de Paly, J. Hecht-Méndez, M. Beck, P. Blum, A. Zell, P. Bayer, Optimization of energy extraction for closed shallow geothermal systems using linear programming, Geothermics 43 (2012) 57–65. doi:10.1016/j.geothermics.2012.03.001.

[8] J. Hecht-Méndez, M. De Paly, M. Beck, P. Bayer, Optimization of energy extraction for vertical closed-loop geothermal systems considering groundwater flow, Energy Conversion and Management 66 (2013) 1–10. doi:10.1016/j.enconman.2012.09.019.

[9] P. Bayer, M. de Paly, M. Beck, Strategic optimization of borehole heat exchanger field for seasonal geothermal heating and cooling, Applied Energy 136 (2014) 445–453. doi:10.1016/j.apenergy.2014.09.029.

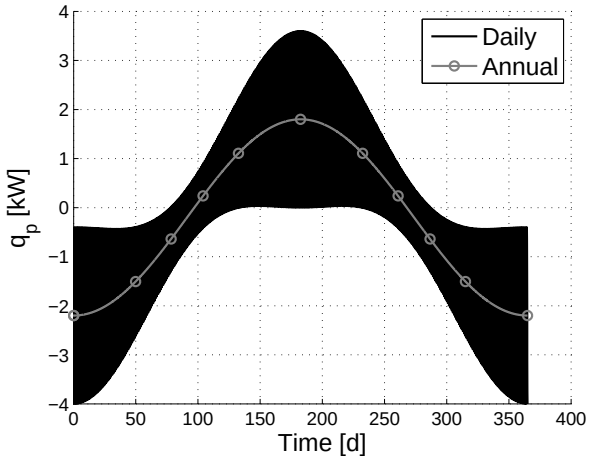

Figure 20: Annual power use including daily variations

[10] L. Laloui, M. Nuth, L. Vulliet, Experimental and numerical investigations of the behaviour of a heat exchanger pile, International Journal for Numerical and Analytical Methods in Geomechanics 30 (8) (2006) 763–781. doi:10.1002/nag.499.

[11] H. Anbergen, J. Frank, L. Müller, I. Sass, Freeze-thaw-cycles on borehole heat exchanger grouts: impact on the hydraulic properties, Geotechnical Testing Journal 37 (4) (2014) 639–651.

[12] S. Erol, B. François, Freeze-thaw damage of grouting materials for borehole heat exchanger: Experimental and analytical evaluations, Geomechanics for Energy and the Environnement 5 (2016) 29–41.

[13] P. Eskilson, Thermal analysis of heat extraction boreholes, Lund University, 1987.

[14] G. Hellström, Ground heat storage : thermal analyses of duct storage systems, Ph.D. thesis, Lund University (1991).

[15] C. Yavuzturk, J. Spitler, A Short Time Step Response Factor Model for Vertical Ground Loop Heat Exchangers, ASHRAE Transactions 105 (2) (1999) 475–485.

[16] M. Philippe, M. Bernier, D. Marchio, Validity ranges of three analytical solutions to heat transfer in the vicinity of single boreholes, Geothermics 38 (4) (2009) 407–413. doi:10.1016/j.geothermics.2009.07.002.

[17] N. Diao, Q. Li, Z. Fang, Heat transfer in ground heat exchangers with groundwater advection, International Journal of Thermal Sciences 43 (12) (2004) 1203–1211. doi:10.1016/j.ijthermalsci.2004.04.009.

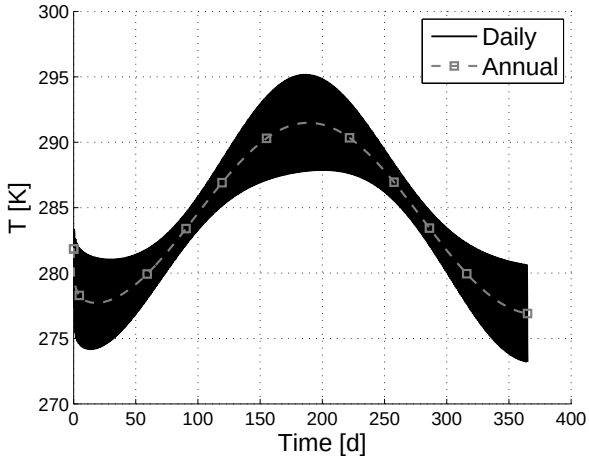

Figure 21: Temperature evolution at the inlet of the pipe (z=100m), daily and annual simulations at different radial positions

[18] L. Lamarche, S. Kajl, B. Beauchamp, A review of methods to evaluate borehole thermal resistances in geothermal heat-pump systems, Geothermics 39 (2) (2010) 187–200. doi:10.1016/j.geothermics.2010.03.003.

[19] S. Erol, M. Hashemi, B. François, Analytical solution of discontinuous heat extraction for sustainability and recovery aspects of borehole heat exchangers, International Journal of Thermal Sciences 88 (2015) 47–58. doi:10.1016/j.ijthermalsci.2014.09.007.

[20] S. Erol, B. François, Thermal stresses in borehole heat exchangers, International Journal for Numerical and Analytical Methods in Geomechanics 39 (2015) 1450–1470. doi:10.1002/nag.

[21] R. Al-Khoury, S. Focaccia, A spectral model for transient heat flow in a double U-tube geothermal heat pump system, Renewable Energy 85 (2016) 195–205. doi:10.1016/j.renene.2015.06.031.

[22] D. Marcotte, P. Pasquier, On the estimation of thermal resistance in borehole thermal conductivity test, Renewable Energy 33 (11) (2008) 2407–2415. doi:10.1016/j.renene.2008.01.021.

[23] R. Beier, J. Acuña, P. Mogensen, B. Palm, Vertical temperature profiles and borehole resistance in a U-tube borehole heat exchanger, Geothermics 44 (2012) 23–32. doi:10.1016/j.geothermics.2012.06.001.

[24] R. Beier, J. Acuña, P. Mogensen, B. Palm, Borehole resistance and vertical temperature profiles in coaxial borehole heat exchangers, Applied Energy 102 (2013) 665–675. doi:10.1016/j.apenergy.2012.08.007.

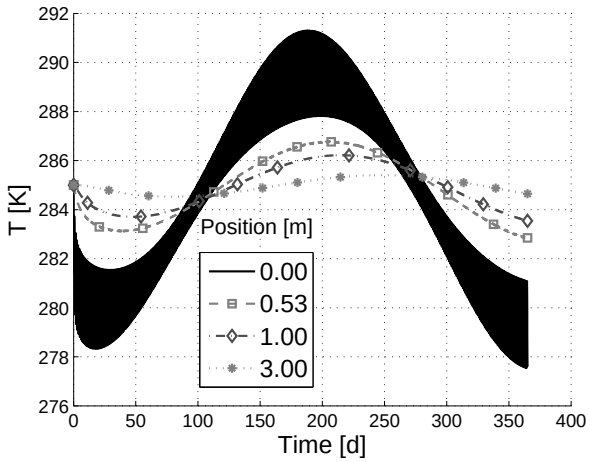

Figure 22: Temperature evolution in an horizontal cross-section (z=80m), daily simulation only

[25] S. Rees, M. He, A three-dimensional numerical model of borehole heat exchanger heat transfer and fluid flow, Geothermics 46 (2013) 1–13. doi:10.1016/j.geothermics.2012.10.004.

[26] D. Bauer, W. Heidemann, H.-J. Diersch, Transient 3D analysis of borehole heat exchanger modeling, Geothermics 40 (4) (2011) 250–260. doi:10.1016/j.geothermics.2011.08.001.

[27] T. Ozudogru, O. Ghasemi-Fare, C. Olgun, P. Basu, Numerical Modeling of Vertical Geothermal Heat Exchangers Using Finite Difference and Finite Element Techniques, Geotechnical and Geological Engineering 33 (2015) 291–306. doi:10.1007/s10706-014-9822-z.

[28] S. Rees, An extended two-dimensional borehole heat exchanger model for simulation of short and medium timescale thermal response, Renewable Energy 83 (2015) 518–526. doi:10.1016/j.renene.2015.05.004.

[29] L. H. Dai, Y. Shang, X. L. Li, S. F. Li, Analysis on the transient heat transfer process inside and outside the borehole for a vertical U-tube ground heat exchanger under short-term heat storage, Renewable Energy 87 (2016) 1121–1129.

[30] R. Al-Khoury, P. Bonnier, R. Brinkgreve, Efficient finite element formulation for geothermal heating systems. part i: Steady state, International journal for numerical methods in engineering 63 (7) (2005) 988–1013.

[31] R. Al-Khoury, P. Bonnier, Efficient finite element formulation for geothermal heating systems. part ii: transient, International journal for numerical methods in engineering 67 (5) (2006) 725–745.

[32] H.-J. Diersch, D. Bauer, W. Heidemann, W. Rühaak, P. Schätzl, Finite element modeling of borehole heat exchanger systems, Part 1. Fundamentals, Computers & Geosciences 37 (8) (2011) 1136–1147. doi:10.1016/j.cageo.2010.08.002.

[33] H.-J. Diersch, D. Bauer, W. Heidemann, W. Rühaak, P. Schätzl, Finite element modeling of borehole heat exchanger systems, Part 2. Numerical simulation, Computers & Geosciences 37 (8) (2011) 1136–1147. doi:10.1016/j.cageo.2010.08.002.

[34] J. Wooszyn, A. Goaś, Experimental verification and programming development of a new MDF borehole heat exchanger numerical model, Geothermics 59 (2016) 67–76. doi:10.1016/j.geothermics.2015.10.006.

[35] D. Bauer, W. Heidemann, H. Müller-Steinhagen, H.-J. Diersch, Experimental investigation of an adsorptive thermal energy storage, International journal of energy research 35 (March) (2011) 135–312–320. doi:10.1002/er.

[36] M. Kummert, M. Bernier, Sub-hourly simulation of residential ground coupled heat pump systems, Building Service Engineering Research and Technology 29 (1) (2008) 27–44. doi:10.1177/0143624407087286.

[37] V. Partenay, P. Riederer, T. Salque, E. Wurtz, The influence of the borehole short-time response on ground source heat pump system efficiency, Energy and Buildings 43 (6) (2011) 1280–1287. doi:10.1016/j.enbuild.2011.01.009.

[38] P. Hein, O. Kolditz, U.-J. Görke, A. Bucher, H. Shao, A numerical study on the sustainability and efficiency of borehole heat exchanger coupled ground source heat pump systems, Applied Thermal Engineering 100 (2016) 421–433.

[39] P. Cui, H. Yang, Z. Fang, Numerical analysis and experimental validation of heat transfer in ground heat exchangers in alternative operation modes, Energy and Buildings 40 (2008) 1060–1066. doi:10.1016/j.enbuild.2007.10.005.

[40] S. Lazzari, A. Priarone, E. Zanchini, Long-term performance of BHE (borehole heat exchanger) fields with negligible groundwater movement, Energy 35 (12) (2010) 4966–4974. doi:10.1016/j.energy.2010.08.028.

[41] R. Al-Khoury, T. Kölbel, R. Schramedei, Efficient numerical modeling of borehole heat exchangers, Computers & Geosciences 36 (10) (2010) 1301–1315. doi:10.1016/j.cageo.2009.12.010.

[42] C. Lee, A modified three-dimensional numerical model for predicting the short-time-step performance of borehole ground heat exchangers, Renewable Energy 87 (2016) 618–627. doi:10.1016/j.renene.2015.10.052.

[43] F. Collin, R. Chambon, R. Charlier, A finite element method for poro mechanical modelling of geotechnical problems using local second gradient models, International journal for numerical methods in engineering 65 (11) (2006) 1749–1772.

[44] P. Gerard, R. Charlier, R. Chambon, F. Collin, Influence of evaporation and seepage on the convergence of a ventilated cavity, Water resources research 44 (5).

[45] F. Collin, X.-L. Li, J.-P. Radu, R. Charlier, Thermo-hydro-mechanical coupling in clay barriers, Engineering Geology 64 (2) (2002) 179–193.

[46] O. Zienkiewicz, R. Taylor, The finite element method, the basis, 5th Edition, McGraw-hill London, 2000.

[47] O. Zienkiewicz, R. Taylor, The finite element method, fluid dynamics, 5th Edition, McGraw-hill London, 2000.

[48] A. N. Brooks, T. J. Hughes, Streamline upwind/petrov-galerkin formulations for convection dominated flows with particular emphasis on the incompressible navier-stokes equations, Computer methods in applied mechanics and engineering 32 (1) (1982) 199–259.

[49] J. Heinrich, P. Huyakorn, O. Zienkiewicz, A. Mitchell, An upwindfinite element scheme for two-dimensional convective transport equation, International Journal for Numerical Methods in Engineering 11 (1) (1977) 131–143.

[50] R. Courant, K. Friedrichs, H. Lewy, On the partial difference equations of mathematical physics, IBM journal of Research and Development 11 (2) (1967) 215–234.

[51] V. Gnielinski, New equations for heat and mass transer in turbulent pipe and channel flow, International Journal of Chemical Engineering 16.

[52] R. Al-Khoury, Computational modeling of shallow geothermal systems, CRC Press, 2011.

[53] L. Ingersoll, O. Zobel, A. Ingersoll, Heat conduction with engineering and geological applications, 1st Edition, International series in pure and applied physics, McGraw-Hill, 1948.

[54] T. Ozudogru, C. Olgun, a. Senol, 3D numerical modeling of vertical geothermal heat exchangers, Geothermics 51 (2014) 312–324. doi:10.1016/j.geothermics.2014.02.005.

[55] K.-J. Bathe, M. Khoshgoftaar, Finite element formulation and solution of nonlinear heat transfer, Nuclear Engineering and Design 51 (3) (1979) 389–401.

[56] W. Wood, R. Lewis, A comparison of time marching schemes for the transient heat conduction equation, International Journal for Numerical Methods in Engineering 9 (3) (1975) 679–689.

[57] S. Signorelli, Geoscientific investigations for the use of shallow low-enthalpy systems, Ph.D. thesis, Diss., Eidgenössische Technische Hochschule ETH Zürich (2004).

[58] M. Fossa, F. Minchio, The effect of borefield geometry and ground thermal load profile on hourly thermal response of geothermal heat pump systems, Energy 51 (0) (2013) 323–329. doi:10.1016/j.energy.2012.12.043.

Appendix A. Force vectors

The out of balance equivalent nodal forces related to the pipe part are computed according to

$$\mathbf{F}_p^e = S \int_{-1}^{1} \rho\, c_p\, \mathbf{W}\, \frac{\partial \mathrm{T}}{\partial t}\, |\mathrm{J}|\, \mathrm{d}z - S \int_{-1}^{1} k \left[\frac{\partial \mathbf{W}}{\partial z}\right] \frac{\partial \mathrm{T}}{\partial z}\, |\mathrm{J}|\, \mathrm{d}z + S \int_{-1}^{1} \mathbf{W} v\, \rho\, c_p\, \frac{\partial \mathrm{T}}{\partial z}\, |\mathrm{J}|\, \mathrm{d}z - P \int_{-1}^{1} \mathbf{W}\, h\, (\mathrm{T}_g - \mathrm{T})\, |\mathrm{J}|\, \mathrm{d}z. \tag{A.1}$$

The exact solution of this equation is provided hereafter, assuming that thermal properties do not depend on temperature and using weighting and shape functions respectively defined in Equations (13)-(17),

$$\begin{aligned}\mathbf{F}_p^e = |\mathbf{J}|\, S\, \rho\, c_p & \begin{bmatrix} \frac{2}{3} - \frac{\beta}{2} & \frac{1}{3} - \frac{\beta}{2} \\ \frac{1}{3} + \frac{\beta}{2} & \frac{2}{3} + \frac{\beta}{2} \end{bmatrix} \cdot \begin{bmatrix} \frac{\partial \tilde{\mathrm{T}}_1}{\partial t} \\ \frac{\partial \tilde{\mathrm{T}}_2}{\partial t} \end{bmatrix} - \frac{S\, k}{2\, |\mathbf{J}|} \begin{bmatrix} 1 & -1 \\ -1 & 1 \end{bmatrix} \cdot \begin{bmatrix} \tilde{\mathrm{T}}_1 \\ \tilde{\mathrm{T}}_2 \end{bmatrix} \\ & + \frac{S\, v\, \rho\, c_p}{2} \begin{bmatrix} -1+\beta & 1-\beta \\ -1-\beta & 1+\beta \end{bmatrix} \cdot \begin{bmatrix} \tilde{\mathrm{T}}_1 \\ \tilde{\mathrm{T}}_2 \end{bmatrix} \\ -P\, h |\mathbf{J}| & \begin{bmatrix} \frac{2}{3} - \frac{1}{2}\beta & \frac{1}{3} - \frac{1}{2}\beta & -\frac{2}{3} + \frac{1}{2}\beta & -\frac{1}{3} + \frac{1}{2}\beta \\ \frac{1}{3} + \frac{1}{2}\beta & \frac{2}{3} + \frac{1}{2}\beta & -\frac{1}{3} - \frac{1}{2}\beta & -\frac{2}{3} - \frac{1}{2}\beta \end{bmatrix} \cdot \begin{bmatrix} \tilde{\mathrm{T}}_1 \\ \tilde{\mathrm{T}}_2 \\ \tilde{\mathrm{T}}_{g1} \\ \tilde{\mathrm{T}}_{g2} \end{bmatrix} \end{aligned} \tag{A.2}$$

where $\tilde{\mathrm{T}}_1$ and $\tilde{\mathrm{T}}_2$ are the nodal temperatures on the pipe side and $\tilde{\mathrm{T}}_{g1}$ and $\tilde{\mathrm{T}}_{g2}$ are the nodal temperatures on the ground side. The out of balance vector related to the ground nodes is defined similarly but only convective exchange

matters. It is equal to

$$\mathbf{F}_g^e = P\,h|\mathbf{J}|\begin{bmatrix} \frac{2}{3}-\frac{1}{2}\beta & \frac{1}{3}-\frac{1}{2}\beta & -\frac{2}{3}+\frac{1}{2}\beta & -\frac{1}{3}+\frac{1}{2}\beta \\ \frac{1}{3}+\frac{1}{2}\beta & \frac{2}{3}+\frac{1}{2}\beta & -\frac{1}{3}-\frac{1}{2}\beta & -\frac{2}{3}-\frac{1}{2}\beta \end{bmatrix}\cdot\begin{bmatrix} \tilde{\mathrm{T}}_1 \\ \tilde{\mathrm{T}}_2 \\ \tilde{\mathrm{T}}_{g1} \\ \tilde{\mathrm{T}}_{g2} \end{bmatrix}. \tag{A.3}$$

Appendix B. Stiffness matrices

The elementary stiffness matrix (size 4×4)is decomposed into different components (sizes 2×2) such that

$$[\mathbf{K}^e]_{4\times4} = \begin{bmatrix} [\mathbf{K}_{pp}]_{2\times2} & [\mathbf{K}_{pg}]_{2\times2} \\ [\mathbf{K}_{gp}]_{2\times2} & [\mathbf{K}_{gg}]_{2\times2} \end{bmatrix}, \tag{B.1}$$

where the subscript p is related to the pipe unknowns $[\tilde{\mathrm{T}}_1 \quad \tilde{\mathrm{T}}_2]^T$ and g to the ground unknowns $[\tilde{\mathrm{T}}_{g1} \quad \tilde{\mathrm{T}}_{g2}]^T$. These components are easily obtained from Equations (A.2) and (A.3) such that,

$$\mathbf{K}_{pp} = |\mathbf{J}|\,\frac{S}{\theta\,\Delta t}\,\rho\,c_p\begin{bmatrix} \frac{2}{3}-\frac{\beta}{2} & \frac{1}{3}-\frac{\beta}{2} \\ \frac{1}{3}+\frac{\beta}{2} & \frac{2}{3}+\frac{\beta}{2} \end{bmatrix} - \frac{S\,k}{2\,|\mathbf{J}|}\begin{bmatrix} 1 & -1 \\ -1 & 1 \end{bmatrix} + \frac{S\,v\,\rho\,c_p}{2}\begin{bmatrix} -1+\beta & 1-\beta \\ -1-\beta & 1+\beta \end{bmatrix}$$
$$-P\,h|\mathbf{J}|\begin{bmatrix} \frac{2}{3}-\frac{1}{2}\beta & \frac{1}{3}-\frac{1}{2}\beta \\ \frac{1}{3}+\frac{1}{2}\beta & \frac{2}{3}+\frac{1}{2}\beta \end{bmatrix}, \tag{B.2}$$

$$\mathbf{K}_{pg} = -P\,h|\mathbf{J}|\begin{bmatrix} -\frac{2}{3}+\frac{1}{2}\beta & -\frac{1}{3}+\frac{1}{2}\beta \\ -\frac{1}{3}-\frac{1}{2}\beta & -\frac{2}{3}-\frac{1}{2}\beta \end{bmatrix}, \tag{B.3}$$

$$\mathbf{K}_{gp} = P\,h|\mathbf{J}|\begin{bmatrix} \frac{2}{3}-\frac{1}{2}\beta & \frac{1}{3}-\frac{1}{2}\beta \\ \frac{1}{3}+\frac{1}{2}\beta & \frac{2}{3}+\frac{1}{2}\beta \end{bmatrix}, \tag{B.4}$$

$$\mathbf{K}_{gg} = P\,h|\mathbf{J}|\begin{bmatrix} -\frac{2}{3}+\frac{1}{2}\beta & -\frac{1}{3}+\frac{1}{2}\beta \\ -\frac{1}{3}-\frac{1}{2}\beta & -\frac{2}{3}-\frac{1}{2}\beta \end{bmatrix}. \tag{B.5}$$